PERGAMON

International Journal of Solids and Structures 36 (1999) 3799–3820

INTERNATIONAL JOURNAL OF SOLIDS and STRUCTURES

An assessment of shell theories for buckling of circular cylindrical laminated composite panels loaded in axial compression

Navin Jaunky, Norman F. Knight Jr.*

Old Dominion University, Norfolk, VA 23529-0247, U.S.A.

Received 16 October 1997; in revised form 27 May 1998

Abstract

Buckling loads of circular cylindrical laminated composite panels are obtained using Sanders–Koiter (e.g. Sanders, 1959; Koiter, 1959), Love (e.g. Love, 1927) and Donnell (e.g. Loo, 1957) shell theories with a first-order, shear-deformation approach and a Rayleigh–Ritz method that accounts for different boundary conditions and material anisotropy. Results obtained using Sanders–Koiter, Love, Donnell shell theories are compared with those obtained from finite element simulations, where the curved panels are modeled using nine-node quadrilateral continuum-based shell elements that are independent of any shell theory. Comparisons with finite element results indicate that Donnell's theory could be in error for some lamination schemes and geometrical parameters.

1. Introduction

Due to their high specific modulus and strength compared to metallic material, fiber-reinforced composite materials offer potential for lighter weight and hence more efficient structures for application in various fields of modern engineering. One such field of modern engineering is aerospace engineering where aerospace structures such as wings or fuselages are mostly assemblies of shell structures. Hence, the analysis of composite shell structures has been of considerable interest to researchers because of its increasing use in the aerospace industry.

Many shell theories developed for thin elastic isotropic circular cylindrical shells are based on the Kirchhoff–Love hypothesis. Since fiber-reinforced composites have a low transverse shear modulus compared to isotropic materials, the Kirchhoff–Love hypothesis of non-deformable normals is not strictly applicable for laminated shell structures. Hence, shell theories accounting

* Corresponding author. Present address: MRJ Technology Solutions, Inc., 303 Heaven's Way, Yorktown, VA 23693-2619, U.S.A. Fax: 001 757 867-6394; E-mail: knight@mrj.com

0020–7683/99/$ - see front matter
PII: S0020–7683(98)00177–2

for transverse shear deformations were developed. Incorporating transverse shear deformation effects through the thickness results in a first-order, shear-deformation (FSDT) theory. Examples of shell theories for circular cylindrical shell with FSDT are extensions of the Sanders–Koiter (e.g. Sanders, 1959; Koiter, 1959); Love (e.g. Love, 1927), and Donnell (e.g. Loo, 1957) shell theories. Leissa (1973) provides an account and comparison of thirteen shell theories with proper assessment of both strain–displacement relations and stress resultants. Recent bibliographies and review papers have also appeared (e.g. Knight and Starnes, 1997; Noor, 1990; Teng, 1996).

These theories involve the thinness assumption while still retaining the first-order, shear-deformation approximation through the shell thickness. Donnell's theory neglects the contribution of the transverse shearing force intensity (Q_y) to the equilibrium of forces in the circumferential direction, while the Sanders–Koiter and Love shell theories include it. For this reason, the Donnell's shell theory is often referred to as Donnell quasi-shallow shell equations (e.g. Brush and Almroth, 1975). Love and Donnell shell theories do not include the contribution of transverse and axial displacement in the twist terms. In view of these differences, it is important to establish the accuracy of these shell theories for composite circular cylindrical shell or panels, where the material could be anisotropic.

Chandrashekara et al. (1995) presents a list of references dealing with contributions made to the linear static stress analysis of composite shell structures. According to Chandrashekara et al. (1995), shell theories with or without transverse shear have been used individually to examine the static, dynamic responses and buckling characteristics of laminated composite circular cylindrical shell structures, and very few researchers have actually studied composite shell structures using different shell theories. Chandrashekara et al. (1995) also provide a list of such references where thermoelastic, dynamic and static responses of bimodulus composite circular cylindrical shell were studied using different shell theories, however these studies do not establish the accuracy of any shell theory.

In order to establish the accuracy of any shell theory, it is important to compare results obtained from each shell theory with results from analyses that are independent of any shell theory. Such a study is found in Leissa (1973) and Chandrashekara et al. (1995). Vibration frequency parameters for isotropic circular cylindrical shell with different length-to-radius and radius-to-thickness ratios determined for various shell theories are presented in Leissa (1973). The frequency parameters according to different shell theories are compared with exact three-dimensional elasticity solutions, and Leissa (1973) found that Donnell's theory could be in error for some geometrical parameters. Chandrashekara et al. (1995) obtained the response of orthotropic circular cylindrical shells and panels under static load using various shell theories, and results are compared with three-dimensional elasticity solutions. Stresses and displacement were compared, and it was found that Donnell's theory could be in error for some lamination schemes and geometrical parameters of the shell or panel.

The accuracy of shell theories for buckling was not assessed by Chandrashekara et al. (1995). Buckling loads for a circular cylindrical shell obtained using different shell theory are presented by Simitses et al. (1985) and Yi-Wei et al. (1997). Buckling loads were obtained for orthotropic cylinders with classical simply support boundary conditions using Donnell's and Sanders theories and were compared to each other by Simitses et al. (1985). Yi-Wei et al. (1997) presents axial buckling loads for a circular cylindrical shell with laminate stacking sequence $[\pm\theta/\pm\theta/\theta]_s$ and showed that differences exist in buckling loads between results obtained using Sanders' equations and Donnell's equation for some values of the fiber winding angle θ. These buckling loads were not compared with results from an analysis which is independent of any shell theory.

The main objective of the present paper is to assess the accuracy of Sanders–Koiter, Love, and Donnell shell theories for buckling analysis using results obtained from finite element analyses. The STAGS finite element code by Brogan et al. (1994) is used where a curved panel is modeled using nine-node quadrilateral continuum-based shell elements which is independent of any shell theory. Results using Sanders–Koiter, Love, and Donnell shell theories are obtained from a Rayleigh–Ritz method where the Ritz functions consist of a circulation function (see Jaunky et al., 1995a) and Legendre polynomials in order to impose different boundary conditions and account for material anisotropy. These shell theories are commonly used because of their simplicity. Buckling loads for laminated and isotropic circular cylindrical curved panels are obtained for different geometrical parameters.

2. Analytical approach

The minimum total potential energy principle energy and a Rayleigh–Ritz solution procedure based on Legendre polynomial function are used to develop a buckling analysis for circular cylindrical panels. Sanders–Koiter, Love, and Donnell shell theories are implemented through the use of 'tracer' coefficients. The analysis method is briefly described in the following sub-sections.

2.1. Strain–displacement relations

The displacement field for a cylindrical shell, according to a first-order, shear-deformation theory is given by

$$\begin{aligned} u(x,y,z) &= u_0(x,y) + z\phi_x(x,y) \\ v(x,y,z) &= v_0(x,y) + z\phi_y(x,y) \\ w(x,y,z) &= w_0(x,y) \end{aligned} \tag{1}$$

where u_0 is the membrane displacement in the x-direction, v_0 is the membrane displacement in the y-direction, w_0 is the out-of-plane transverse displacement in the z-direction, positive ϕ_x and ϕ_y are the cross-sectional clockwise rotations around the y- and x-axes, respectively. The axial coordinate is x, the circumferential coordinate is y, and the thickness coordinate normal to the shell surface is z.

According to FSDT, cross-sections normal to the reference plane before deformation are assumed to remain planar but not necessarily normal to mid-surface after deformation. A differential element of a cylindrical shell segment with the coordinate axes, notations and sign convention is given in Fig. 1. The circumferential coordinate θ is replaced by $y = R\theta$, where R is the radius of the cylindrical shell segment. Noting that $\partial y = R\,\partial\theta$, the linear strain–displacement relations (see Bert and Birman, 1988) can be written as;

$$\varepsilon_{x\mathrm{L}} = \varepsilon_x^0 + z\kappa_x$$

$$\varepsilon_{y\mathrm{L}} = \varepsilon_y^0 + z\kappa_y$$

$$\gamma_{xy\mathrm{L}} = \gamma_{xy}^0 + z\kappa_{xy}$$

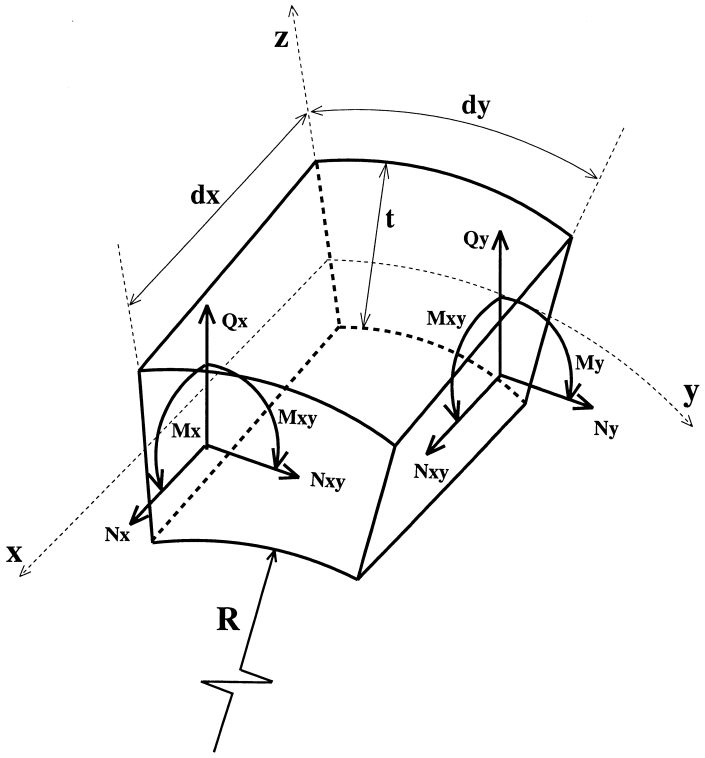

Fig. 1. Sign convention for cylindrical shell differential element.

$$\gamma_{xz\mathrm{L}} = \gamma^0_{xz}$$
$$\gamma_{yz\mathrm{L}} = \gamma^0_{yz} \tag{2}$$

where the mid-plane strains ε^0_x, ε^0_y, $^0_{xy}$, and the changes in curvature κ_x, κ_y, κ_{xy} and the transverse shear strains γ^0_{xz}, γ^0_{xy} are given by

$$\varepsilon^0_x = \frac{\partial u_0}{\partial x}$$
$$\varepsilon^0_y = \frac{\partial v_0}{\partial y} + \frac{w_0}{R}$$
$$\gamma^0_{xy} = \frac{\partial u_0}{\partial y} + \frac{\partial v_0}{\partial x}$$
$$\kappa_x = \frac{\partial \phi_x}{\partial x}$$
$$\kappa_y = \frac{\partial \phi_y}{\partial y}$$

$$\kappa_{xy} = \frac{\partial \phi_x}{\partial y} + \frac{\partial \phi_y}{\partial x} + \frac{C_2}{2R}\left(\frac{\partial v_0}{\partial x} - \frac{\partial u_0}{\partial y}\right)$$

$$\gamma^0_{xz} = \phi_x + \frac{\partial w_0}{\partial x}$$

$$\gamma^0_{yz} = \phi_y + \frac{\partial w_0}{\partial y} - C_1 \frac{v_0}{R} \tag{3}$$

The subscript 'L' denotes linear strain component. Here C_1 and C_2 are 'tracer' coefficients used to implement different shell theories or strain–displacement relations. Accordingly when

- $C_1 = C_2 = 1$, the first approximation of Sanders–Koiter shell theory (see Sanders, 1959; Koiter, 1959) is obtained.
- $C_1 = 1$, $C_2 = 0$, Love's shell theory (see Love, 1927) including transverse shear deformations is obtained.
- $C_1 = 0$ and $C_2 = 0$, Donnell's shell theory (see Loo, 1957) including transverse shear deformation is obtained.

The nonlinear components of the strain–displacement relations for a circular cylindrical shell or panel (see Stein, 1986), are

$$\varepsilon_{x\mathrm{NL}} = \frac{1}{2}(v^2_{0,x} + w^2_{0,x})$$

$$\varepsilon_{y\mathrm{NL}} = \frac{1}{2}\left[u^2_{0,y} + \left(w_{0,y} - \frac{v_0}{R}\right)^2\right]$$

$$\gamma_{xy\mathrm{NL}} = -u_{0,y}\left(v_{0,y} + \frac{w_0}{R}\right) - v_{0,x}u_{0,x} + w_{0,x}\left(w_{0,y} - \frac{v_0}{R}\right) \tag{4}$$

where a comma is used to indicate differentiation with respect to the next subscripted independent variable. For example $v_{0,x}$ denotes $\partial v_0/\partial x$. The subscript 'NL' denotes nonlinear strain component. Equations (4) are obtained after neglecting higher-order terms for the cross-sectional rotations since in the prebuckled state the cross-sectional rotations tend to zero, the nonlinear terms in the transverse shear strains, and the z/R terms.

2.2. Rayleigh–Ritz method

The physical domain (x, y) of the curved panel mid-surface is transformed to a computational domain (ξ, η) using bilinear shape functions (see Jaunky et al., 1995a), and the displacements of the panel are then expressed in terms of the natural coordinates (ξ, η). As such, the computational domain is a square domain where ξ and η take on values of ± 1. The components of the displacement vector are three translations $(D_1, D_2, D_3 = u_0, v_0, w)$ and two bending rotations $(D_4, D_5 = \phi_x, \phi_y)$ when considering transverse shear deformation effects. Each displacement component is approxi-

mated independently by a different Ritz function. The approximation for the ith component of the displacement vector is given by

$$D_i(\xi,\eta) = \sum_{j=1}^{N} a_{ij} d_{ij}$$

$$= \sum_{j=1}^{N} a_{ij} \Gamma_i(\xi,\eta) f_j(\xi,\eta) \quad \text{for } i = 1,2,3,4,5 \tag{5}$$

where d_{ij} represents the jth term in the N-term approximation for the ith displacement component, a_{ij} are unknown coefficients to be determined, and $\Gamma_i(\xi,\eta)$ are the circulation functions. The circulation functions are used to impose different boundary conditions along the edge of the panel. Each term Γ_i is the product of four functions, and each function is the equation of an edge of the computational domain raised to an independent exponent for each displacement component. Thus, the circulation functions for a quadrilateral domain are

$$\Gamma_i(\xi,\eta) = (1-\eta)^{p_i}(1-\xi)^{q_i}(1+\eta)^{r_i}(1+\xi)^{s_i} \tag{6}$$

The exponents, p_i, q_i, r_i, and s_i can be used to imposed different boundary conditions. For example, consider the edge ($\eta = 1$), the value of p_i will determine the value of the displacement component D_i on edge ($\eta = 1$). Accordingly when

- $p_i = 0$, D_i is free on edge ($\eta = 1$).
- $p_i = 1$, D_i is constraint on edge ($\eta = 1$).

Hence the values of the exponents p_i, q_i, r_i and s_i can be used to impose different geometric boundary conditions as discussed by Jaunky et al. (1995a).

The term f_j in eqn (5) is a polynomial function in ξ and η, and since Legendre polynomial (see Andrews, 1985) are herein considered, the function term f_j is defined as

$$f_j = P_{m_j}(\xi) P_{n_j}(\eta)$$

$$m_j, n_j = \begin{cases} (0,0),(0,1),(0,2),\ldots,(0,N) \\ (1,0),(1,1),(1,2),\ldots,(1,N) \\ \qquad\vdots \\ (N,0),(N,1),(N,2),\ldots,(N,N) \end{cases} \tag{7}$$

where $P_{m_j}(\vartheta)$ denotes a Legendre polynomial of degree m_j in variable ϑ and is defined over the interval, $-1 \leqslant \vartheta \leqslant 1$. Some properties of these polynomials can be exploited for computational efficiency in setting up the stiffness matrices as discussed in the Appendix. Legendre polynomials are preferred over a simple polynomial function (e.g. $f_j = \xi^{m_j}\eta^{n_j}$) since Legendre polynomials are orthogonal, hence lead to better convergence characteristics, and do not lead to ill-conditioning of stiffness matrices for large values of N (see Jaunky, 1995). Figure 2 (taken from Jaunky, 1995) illustrates the convergence characteristic of Legendre polynomials compared to a simple polynomial series ($\xi^{m_j}\eta^{n_j}$) for a simply supported isotropic 45°-skewed plate subjected to axial compression. The Ritz functions with Legendre polynomials gives results that converge faster than the Ritz functions with a simple polynomial series. The type of Ritz functions used also account for anisotropic material properties as shown by Jaunky et al. (1995a, b).

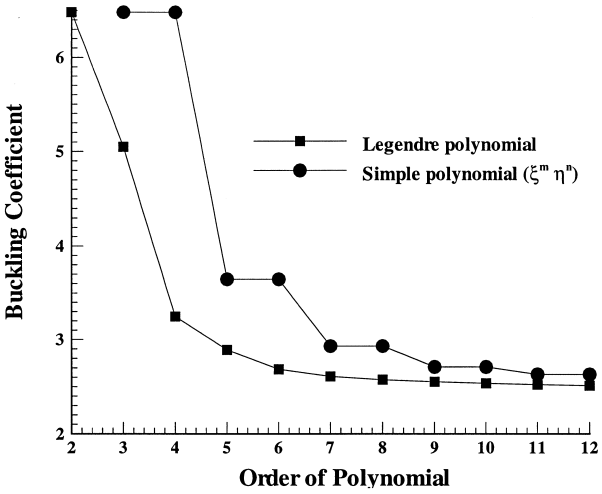

Fig. 2. Convergence of buckling coefficient with increasing order of polynomial for a simply supported isotropic 45° skewed plate subjected to axial compression (from Jaunky, 1995).

2.3. The minimum total potential energy principle

The critical stresses are determined on the basis of the principle that during buckling the elastic strain energy stored in the structure is equal to the work done by the applied load (see Stein and Neff, 1947; Stein and Batdorf, 1947). For a cylindrical composite panel, the elastic strain energy (U) is

$$U = \frac{1}{2}\int_A \{\varepsilon\}^T \begin{bmatrix} A_{ij} & B_{ij} & 0 \\ B_{ij} & D_{ij} & 0 \\ 0 & 0 & C_{pq} \end{bmatrix} \{\varepsilon\}\, \mathrm{d}A \tag{8}$$

where

$$\{\varepsilon\}^T = \{\varepsilon_x^0 \quad \varepsilon_y^0 \quad \gamma_{xy}^0 \quad \kappa_x \quad \kappa_y \quad \kappa_{xy} \quad \gamma_{xz} \quad \gamma_{yz}\}^T \tag{9}$$

and is given by eqn (3). A_{ij}, B_{ij}, D_{ij}, and C_{pq} are the extensional, coupling, bending, and transverse shear stiffness coefficients, respectively.

Considering a linear buckling analysis with a prescribed uniform in-plane prestress state, the work done (W_d) by the applied load can be written as

$$W_\mathrm{d} = \int_A (\bar{N}_x \varepsilon_{x\mathrm{NL}} + \bar{N}_y \varepsilon_{y\mathrm{NL}} + \bar{N}_{xy} \gamma_{xy\mathrm{NL}})\, \mathrm{d}A \tag{10}$$

where the nonlinear strains $\varepsilon_{x\mathrm{NL}}$, $\varepsilon_{y\mathrm{NL}}$, and $\gamma_{xy\mathrm{NL}}$ are given by eqn (4) and $\bar{N}_x$, $\bar{N}_y$, and $\bar{N}_{xy}$ are the prescribed in-plane prestress state. $\bar{N}_x$, $\bar{N}_y$, and $\bar{N}_{xy}$ can be written as

$$\bar{N}_{xy} = \lambda N_1$$

$$\bar{N}_{xy} = \lambda N_2$$
$$\bar{N}_{xy} = \lambda N_{12} \tag{11}$$

where λ is a factor to be determined. N_1, N_2, and N_{12} may be design or reference loads.

Hence at buckling

$$U = W_{\mathrm{d}} \tag{12}$$

The Ritz functions defined in eqn (5) can be substituted in eqn (12) to yield an expression of the form

$$\frac{1}{2}\sum_{i=1}^{N}\sum_{j=1}^{N}\mathbf{X}_i^T\mathbf{K}_{ij}\mathbf{X}_j = \frac{\lambda}{2}\sum_{i=1}^{N}\sum_{j=1}^{N}\mathbf{X}_i^T\mathbf{G}_{ij}\mathbf{X}_j \tag{13}$$

where $\mathbf{K}_{ij}$ and $\mathbf{G}_{ij}$ are the linear stiffness matrix and geometric stiffness matrix, respectively. $\mathbf{X}_i$ is the column vector consisting of the unknown Ritz coefficients a_{ij} of eqn (5) to be determined. The linear stiffness and geometric stiffness matrices are obtained by analytical integration as discussed in the Appendix in order to exploit computational efficiency offered by the Legendre polynomials. Detailed derivation of the Rayleigh–Ritz formulation is given by Jaunky (1995). Minimizing eqn (13) with respect to $\mathbf{X}_i$ leads to

$$\sum_{i=1}^{N}\sum_{j=1}^{N}(\mathbf{K}_{ij}-\lambda\mathbf{G}_{ij})\mathbf{X}_j = 0 \tag{14}$$

which is an eigenvalue problem. The eigenvalues and eigenvectors of the system of equation can be found by using an eigenvalue solver (e.g., power iteration, QR-iteration). In this case, the minimum eigenvalue is the critical load factor (λ_{cr}), the critical load is $N_{\mathrm{cr}} = \lambda_{\mathrm{cr}} \times (N_1, N_2, N_{12})$, and the eigenvector $\mathbf{X}_j$ corresponding to the minimum eigenvalue is the buckling mode shape. Note that while these equations have a form similar to those for a finite element analysis, the vector of unknown $\mathbf{X}_j$ represents a set of unknown coefficients rather than nodal degrees of freedom. Furthermore the symbol Σ means summation rather than assembly as in a finite element approach.

3. Numerical results

Numerical results are presented for anisotropic and isotropic circular cylindrical panels obtained using the buckling analysis described herein. These analytical results are compared with results obtained from the finite element code STAGS [see Brogan et al. (1994)]. The finite element model consists of a mesh of 30×30 nine-node quadrilateral continuum-based shell elements accounting for transverse shear flexibilities. This nine-node quadrilateral continuum-based shell element is known as the 480 Element in the STAGS finite element code, and its formulation is independent of any shell theory. Park and Stanley (1986) give the formulation of the element. In the STAGS finite element analysis, the prebuckling stress state is also prescribed as a uniform in-plane prestress state.

The anisotropic panel has a laminate stacking sequence of $[\pm\theta/\pm\theta/\theta]_{\mathrm{s}}$ with nominal mechanical properties of $E_{11} = 13.75$ Msi, $E_{22} = 1.03$ Msi, $G_{12} = G_{13} = G_{23} = 0.42$ Msi and $\nu_{12} = 0.25$. The

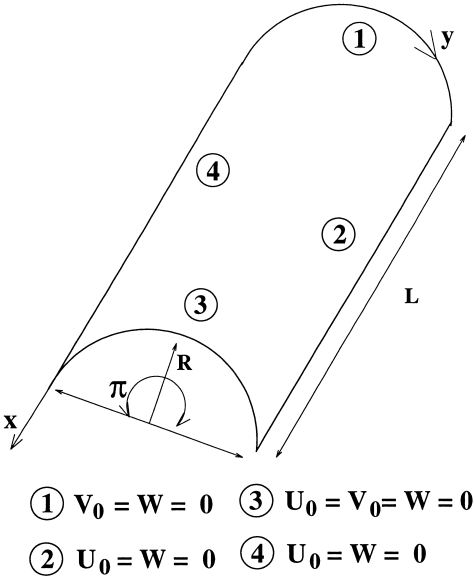

Fig. 3. Geometry of curved panel with simply support boundary conditions (boundary conditions 1).

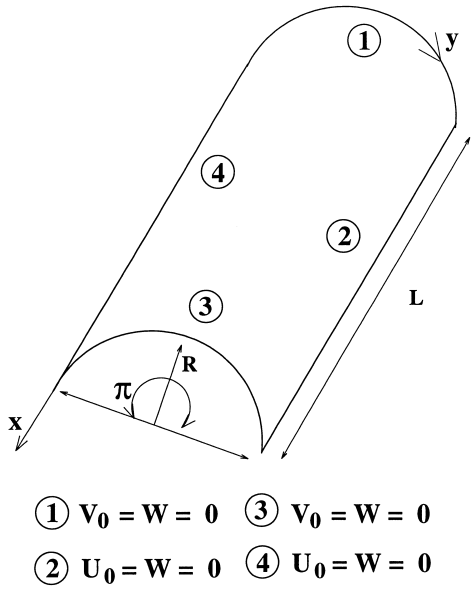

Fig. 4. Geometry of curved panel with classical simply support boundary conditions (boundary conditions 2).

isotropic material has nominal mechanical properties of $E_{11} = 10.0$ Msi and $v_{12} = 0.30$. The geometry of the curved panel is shown in Figs 3 and 4 where the angle subtended by the arc length is π radians, and the geometric boundary conditions are also shown. The panel is considered to be

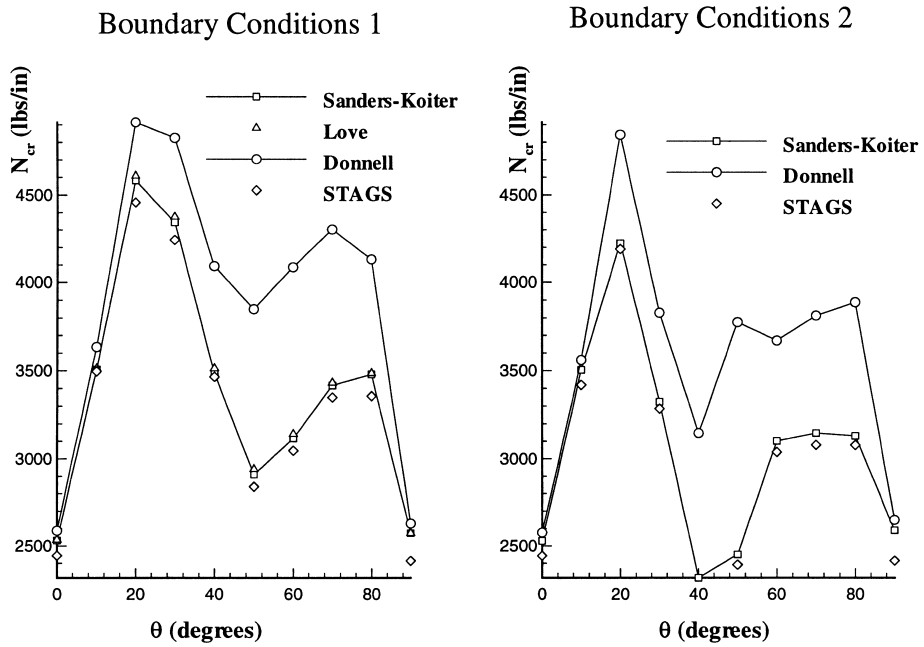

Fig. 5. Comparisons of buckling loads for curved panel from different theories for various winding angle θ in $[\pm\theta/\pm\theta/\theta]_s$ laminate.

simply supported since no bending rotations are constrained on its edges. Two types of simply supported boundary conditions are considered as shown in Figs 3 and 4. The boundary conditions shown in Fig. 4 are the classical simply support boundary conditions which would be obtained by using a Fourier series to approximate the displacement field. Results are presented for curved panels subjected to axial compression with different values of the radius-to-thickness ratio (R/t) and different values of the length-to-radius ratio (L/R).

3.1. Buckling of anisotropic curved panel

The anisotropic curved panel is 60.0-in long with a radius of 6.0 in. Each ply in the $[\pm\theta/\pm\theta/\theta]_s$ laminate is 0.012-in thick. This panel has geometric parameters, $R/t = 50$ and $L/R = 10$. Critical buckling loads for this panel are computed using Sanders–Koiter, Love, and Donnell shell theories and also using STAGS for fiber winding angle in the range $0^\circ \leqslant \theta \leqslant 90^\circ$. The buckling loads were obtained using Legendre polynomials up to the 13th-order ($N = 13$). For the case $\theta = 90^\circ$, Legendre polynomials up to 20th-order ($N = 20$) were used. These buckling loads were obtained for boundary conditions 1 and 2 and are compared in Fig. 5 for different values of fiber winding angle θ.

Considering boundary conditions 1, the results obtained using Love's shell theory are very close to that obtained using Sanders–Koiter shell theory. The STAGS finite element result are also in good agreement with those obtained using Love's and Sanders–Koiter shell theories. The results obtained using Donnell's shell theory correlate well with those obtained by Love's and Sanders–

Koiter shell theories for θ between 0 and 10°. For $\theta > 10°$, Donnell's shell theory overestimates the buckling loads compared to either Sanders–Koiter or Love's shell theory. The difference in buckling loads between those obtained by Sanders–Koiter and Donnell's theories is largest for the range of winding angle given by $50° \leqslant \theta \leqslant 70°$. Above $\theta = 70°$, the difference between the buckling loads obtained by Sanders–Koiter and Donnell shell theories decreases, and at $\theta = 90°$ the loads obtained using Donnell's and Sanders–Koiter shell theories are again close to each other. The buckling loads for anisotropic curved panel obtained using boundary condition 2 has the same trend in the difference between loads obtained using Donnell's theory and Sanders–Koiter's theory.

According to Brush and Almroth (1975), Donnell's theory gives accurate results for cylindrical panels that are relatively flat before deformation and for complete cylindrical shells whose displacement components in the deformed configuration are rapidly varying functions of the circumferential coordinate. Such shells are sometimes termed 'quasi-shallow' shells. The buckling mode shapes for boundary condition 1 obtained from STAGS are shown with exaggerated displacement amplitudes in Fig. 6 for various values of θ. For $\theta = 0$ and 90°, there are more than two half-waves in the circumferential direction. Hence, the buckling loads obtained by Donnell's theory are in good agreement with the other results. For $\theta = 10°$, there are still more than two half-waves on part of the panel and therefore, the result from Donnell's theory is still in agreement with the other results. For $\theta = 20$ and 30°, only one half-wave in the circumferential direction is present, and for $\theta = 40$, 50, 60 and 70°, there are no half-waves in the circumferential direction. Therefore, for these values of θ, the results obtained by Donnell's theory are not expected to be in good agreement with the results predicted by the other shell theories. For $\theta = 80°$, the deformation pattern is more in a skewed direction rather than along the circumferential direction, therefore the result obtained by Donnell's theory is not in agreement with the results predicted by the other shell theories.

These results indicate that Donnell's theory could be in error depending on the degree of orthotropy and anisotropy of the laminate $[\pm\theta/\pm\theta/\theta]_s$. Parameters for the membrane and flexural orthotropy and anisotropy are defined by Nemeth (1994) and given by

$$\mu = \frac{A_{11}A_{22} - A_{12}^2 - 2A_{12}A_{66} + 2A_{16}A_{26}}{2[(A_{11}A_{66} - A_{16}^2)(A_{22}A_{66} - A_{26}^2)]^{1/2}}$$

$$\gamma_m = \frac{A_{11}A_{26} - A_{12}A_{16}}{[(A_{11}A_{66} - A_{16}^2)^3(A_{22}A_{66} - A_{26}^2)]^{1/4}}$$

$$\delta_m = \frac{A_{22}A_{16} - A_{12}A_{26}}{[(A_{11}A_{66} - A_{16}^2)(A_{22}A_{66} - A_{26}^2)^3]^{1/4}}$$

$$\beta = \frac{(D_{12} + 2D_{66})}{(D_{11}D_{22})^{1/2}}$$

$$\gamma_b = \frac{D_{16}}{(D_{11}^3 D_{22})^{1/4}}$$

$$\delta_b = \frac{D_{26}}{(D_{22}^3 D_{11})^{1/4}} \tag{15}$$

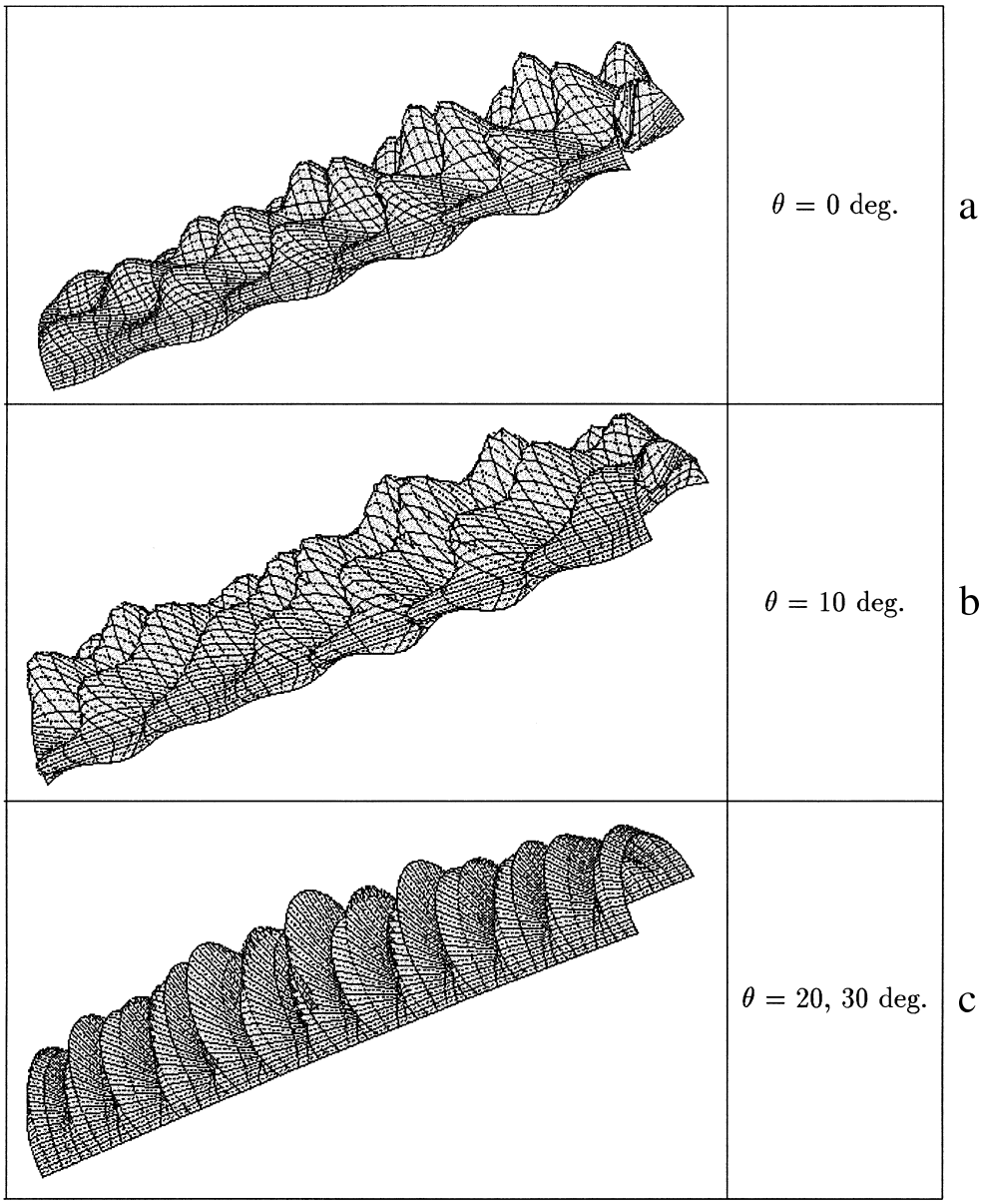

Fig. 6. Buckling mode shape of curved panel for different winding angle θ in $[\pm\theta/\pm\theta/\theta]_s$ laminate.

where μ, γ_m, and δ_m are the membrane orthotropy and anisotropy parameters, respectively and β, γ_b, and δ_b are the flexural orthotropy and anisotropy parameters, respectively. A_{ij} and D_{ij} are the membrane and bending stiffness coefficients (e.g. Jones, 1975). Table 1 gives the values of these parameters and also the percentage difference between buckling loads obtained from Sanders–

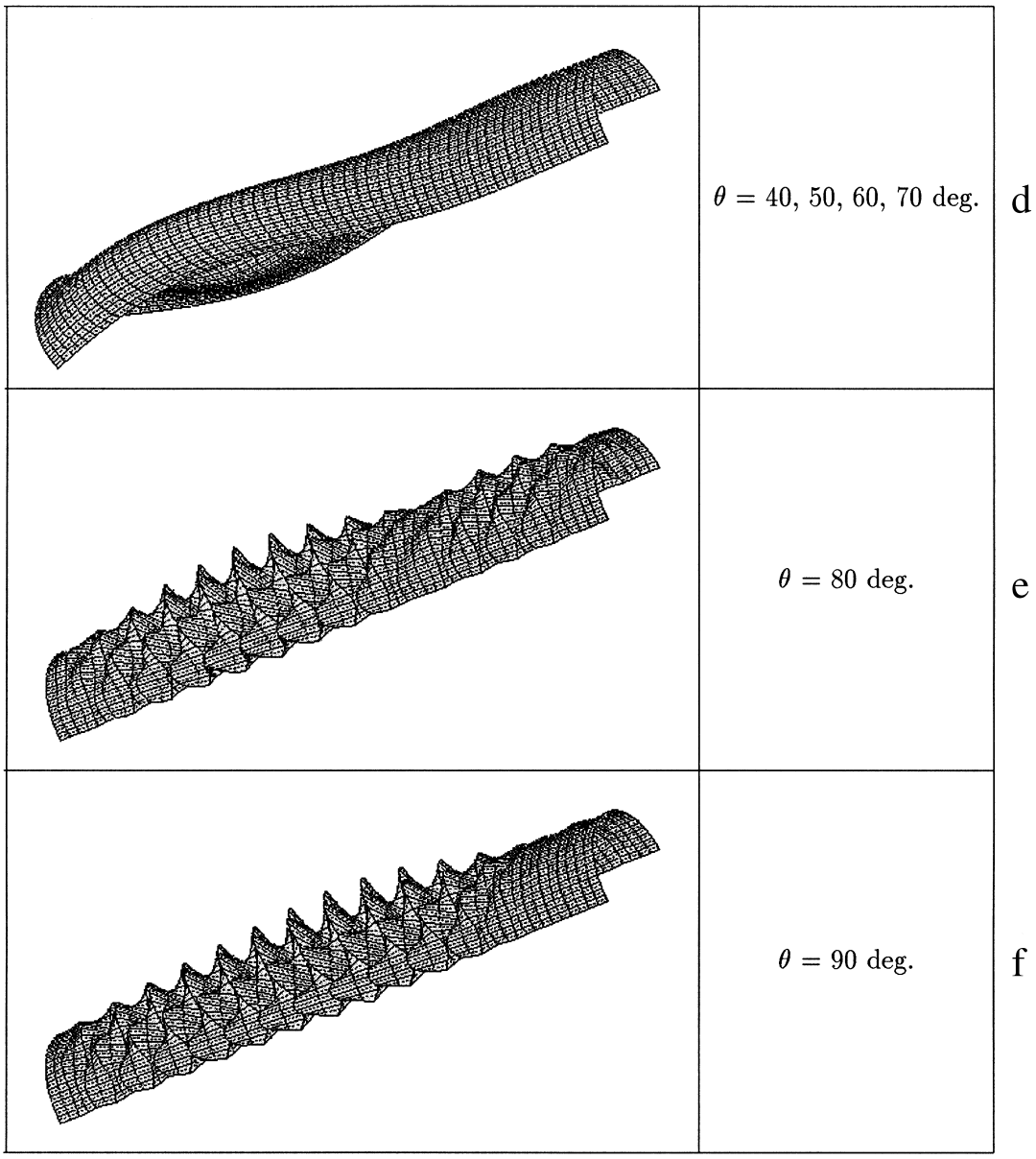

Fig. 6—continued.

Koiter and Donnell shell theories and from Sanders–Koiter's shell theory and STAGS for boundary condition 1. The percentage difference in buckling loads between Donnell's theory and Sanders–Koiter shell theory is

$$\Delta_{\text{don}} = (\lambda_{\text{s-k}} - \lambda_{\text{don}})/\lambda_{\text{don}} \tag{16}$$

and the percentage difference in buckling loads between STAGS and Sanders–Koiter theory is

Table 1
Membrane and flexural parameters for orthotropy and anisotropy of the curved panel

θ (°)	μ	γ_m	δ_m	β	γ_b	δ_b	Δ^*_{don} (%)	Δ^*_{stags} (%)
0	4.41	0.0	0.0	0.29	0.0	0.0	−1.7	3.6
10	2.13	−0.01	0.28	0.59	0.09	0.01	−1.4	0.3
20	0.46	−0.003	0.20	1.37	0.17	0.07	−6.7	2.8
30	−0.27	0.008	0.11	2.10	0.22	0.15	−9.9	2.3
40	−0.55	0.02	0.05	2.44	0.23	0.21	−14.7	0.6
50	−0.55	0.05	0.02	2.44	0.21	0.23	−24.4	2.4
60	−0.27	0.11	−0.008	2.10	0.15	0.22	−23.7	2.3
70	0.46	0.20	−0.003	1.37	0.07	0.17	−20.5	2.0
80	2.13	0.28	−0.01	0.59	0.01	0.09	−15.8	3.6
90	4.41	0.0	0.0	0.29	0.0	0.0	−2.1	6.5

* Δ_{don} and Δ_{stags} for boundary conditions 1.

$$\Delta_{\text{stags}} = (\lambda_{\text{s–k}} - \lambda_{\text{stags}})/\lambda_{\text{stags}} \tag{17}$$

For $\theta = 0$ and 90°, the anisotropy parameters are all zero. For $10^\circ \leqslant \theta \leqslant 80^\circ$, at least one of the anisotropy parameters is non-zero. These orthotropy and anisotropy parameters seem to affect the buckling mode shape of this anisotropic panel with laminate stacking sequence $[\pm\theta/\pm\theta/\theta]_s$ for the given R/t ($R/t = 50$) and L/R ($L/R = 10$) ratios.

3.2. Buckling of curved panel with different R/t ratio

Buckling loads for curved panels with a $[\pm 70/\pm 70/70]_s$ laminate and with isotropic material are obtained using Sanders–Koiter and Donnell shell theories for different values of the R/t ratio. This panel is 60.0-in long, and the angle subtended by the arc length is π radians. Results are shown in Table 2 for the curved panel with boundary condition 1, where the R/t ratio is varied while keeping the radius constant ($R = 6$ in). In Table 3, results for curved panel with boundary condition 1 are presented where the R/t ratio is varied while keeping the thickness of the panel constant ($t = 0.24$ in). Results from the present analysis were obtained with $N = 15$.

The buckling loads presented in Table 2 show about 20–25% difference in buckling load between Sanders–Koiter and Donnell shell theories for R/t ratio up to 100 for the anisotropic laminate. For $R/t = 200$, there is a 6.7% difference, and for $R/t = 600$ there is a 3.5% difference. For the isotropic panel, a considerable difference of 20.04% is shown in buckling loads from Sanders–Koiter and Donnell shell theories for $R/t = 25$. This difference is 10.09% for $R/t = 50$, and the difference is about 5% or less for $R/t = 100$ and 200. For $R/t = 600$, the difference between $\lambda_{\text{s–k}}$ and λ_{don} is less than 1%. The results obtained using Sanders–Koiter are also in good agreement with those obtained using STAGS finite element code.

The buckling loads presented in Table 3 indicate that there is considerable difference in buckling loads (about 20%) from Sanders–Koiter and Donnell theory only for $R/t = 25$ for both the anisotropic and isotropic panels. When R/t is 50, the difference is 8.1 and 3.7% for the anisotropic

Table 2
Buckling loads for curved panel for different R/t ratio with $R = 6.0$ in and $L/R = 10$

t (in)	R/t	λ_{s-k} (lbs/in)	λ_{love} (lbs/in)	λ_{don} (lbs/in)	λ_{stags} (lbs/in)	Δ_{don} (%)	Δ_{stags} (%)
$[\pm 70/\pm 70/70]_s$ laminate							
0.24	25	12,000.0	12,100.0	16,000.0	11,579.0	−25.0	3.6
0.12	50	3416.1	3431.6	4289.9	3349.1	−20.3	2.0
0.06	100	920.2	921.8	1103.1	910.3	−19.9	1.1
0.03	200	261.7	261.8	280.7	260.3	−6.7	0.5
0.01	600	30.79	30.79	31.91	30.47	−3.5	1.0
Isotropic							
0.24	25	42,441.2	42,740.2	53,080.5	41,945.4	−20.04	1.1
0.12	50	12,438.6	12,486.0	13,834.1	12,360.0	−10.09	0.6
0.06	100	3367.2	3373.7	3549.9	3358.8	−5.12	0.2
0.03	200	873.6	874.4	905.3	876.4	−3.66	−0.3
0.01	600	99.75	99.75	100.7	99.73	−0.94	0.02

Table 3
Buckling loads for curved panel for different R/t ratio with $t = 0.24$ in and $L = 60$ in

R (in)	R/t	L/R	λ_{s-k} (lbs/in)	λ_{don} (lbs/in)	λ_{stags} (lbs/in)	Δ_{don} (%)	Δ_{stags} (%)
$[\pm 70/\pm 70/70]_s$ laminate							
6.0	25	10.0	12,000.0	16,000.0	11,579.0	−25.0	3.6
12.0	50	5.0	8359.7	9105.9	8168.2	−8.10	2.3
24.0	100	2.5	4685.8	4810.2	4585.2	−2.60	2.2
48.0	200	1.25	2475.8	2475.9	2349.7	−0.003	5.3
144.0	600	0.417	774.2	774.2	757.4	−0.0	2.2
Isotropic							
6.0	25	10.0	42,441.2	53,080.5	41,945.4	−20.04	1.1
12.0	50	5.0	27,194.7	28,259.2	27,020.0	−3.7	0.6
24.0	100	2.5	14,336.0	14,378.4	14,204.4	−1.8	0.9
48.0	200	1.25	7243.3	7243.3	7222.13	−0.0	0.3
144.0	600	0.417	2421.1	2421.1	2424.2	−0.0	−0.1

and isotropic panel, respectively. For the other R/t ratios, the difference in buckling loads is less than 3% with the difference being zero or very close to zero for $R/t = 200$ and 600. Results obtained using Sanders–Koiter theory are also in good agreement with those obtained using STAGS.

Thus, the curved panel shows different responses to Donnell shell theory for the same R/t ratio, but depends on the value of the radius R. The $1/R$ terms in eqn (3) determine the influence of the coupling between the out-of-plane and in-plane displacements in the shell buckling. As the radius R increases, the coupling decreases and hence the results from Donnell's theory tend to agree with Sanders–Koiter's theory. Isotropy seems to influence Donnell's theory, since the difference in buckling loads from Sanders–Koiter and Donnell's shell theories for the isotropic panel are less than those of the anisotropic panel for the cases considered.

The contour plots of the mode shape of the radial displacement (w_0) obtained from the buckling analysis using Sanders–Koiter theory for the anisotropic panel for different R/t ratios with $R = 6.0$ in are shown in Fig. 7. The curved panel is shown in a planform view in Fig. 7. Only the mode shape for $R/t = 600$ has more than two half-waves in the curved direction, hence, the results of Donnell's theory and Sanders–Koiter are close to each other as expected.

3.3. *Buckling of curved panel with different* L/R *ratio*

Buckling loads for curved panels with laminate $[\pm 70/\pm 70/70]_s$ and isotropic material are obtained using Sanders–Koiter and Donnell shell theories for different R/t ratio, with $R = 6.0$ in. The panel has the same arc length and boundary conditions as the one described in Fig. 3. Results are shown in Table 4 and 5. In Table 4, the R/t ratio is 600 ($t = 0.01$), and in Table 5, the R/t ratio is 25 ($t = 0.24$). The L/R ratio is varied while keeping the radius R constant at 6.0 in. Results from the present analysis were obtained with $N = 15$.

The buckling loads presented in Table 4 for the anisotropic panel show differences in results from Sanders–Koiter and Donnell shell theories between 3.5 and 5.7% for L/R ratios between 15 and 8. For $L/R = 3$ and 5, the difference in buckling loads is about 2%, and for $L/R = 1$, the difference is zero. The difference in buckling loads from Sanders–Koiter and Donnell shell theories for the isotropic panel is 1.8% or less for all the L/R ratios considered. The difference decreases as the L/R ratio decreases. At $L/R = 1$, the difference is zero. The results obtained using Sanders–Koiter shell theory are in good agreement with those obtained using the STAGS finite element code.

The buckling loads presented in Table 5 for the anisotropic, show large difference in buckling loads from Sanders–Koiter and Donnell shell theories for L/R ratio up to five. The difference in buckling loads is 7.6% for $L/R = 3$ and is negligible for $L/R = 1$. For the isotropic panel, the difference in buckling loads from the Sanders–Koiter and Donnell shell theories is large up to $L/R = 8$. For $L/R = 3$ and 5, the difference in buckling loads from the Sanders–Koiter and Donnell shell theories is 6.2 and 3.8%, respectively, for the isotropic panel. The difference in buckling loads is 1.1% for $L/R = 1$.

The difference in buckling loads from the Sanders–Koiter and Donnell shell theories is less for the isotropic panel than for the anisotropic panel. Anisotropy seems to affect the result obtained from Donnell's shell theory for panels with very large R/t and L/R ratios. For thick panels ($R/t = 25$), the difference in buckling loads is large for isotropic and anisotropic panels with large

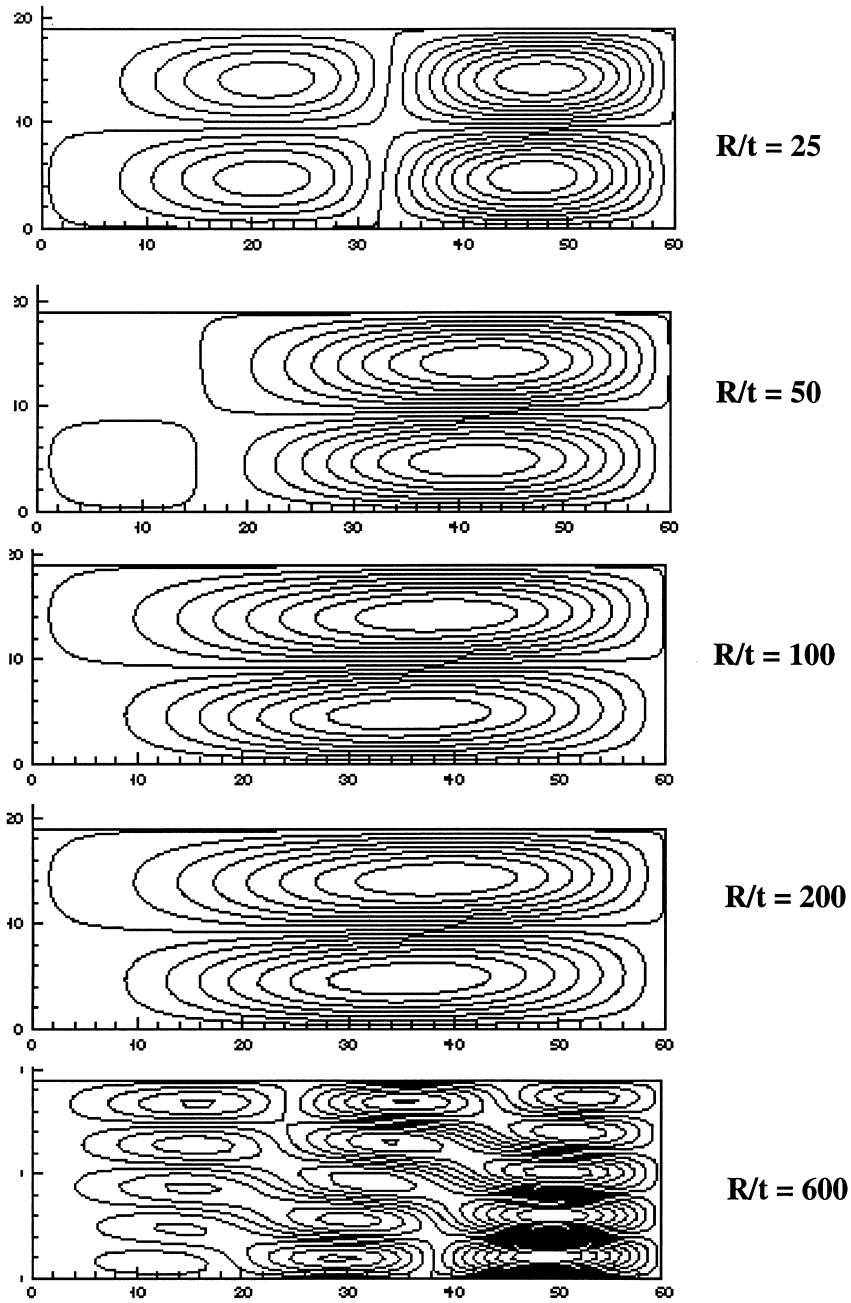

Fig. 7. Buckling mode shapes for $[\pm 70/\pm 70/70]_s$ laminate with different R/t ratios with $R = 6.0$ in.

Table 4
Buckling loads for curved panel with different L/R ratio for $t = 0.01$ in, $R = 6.0$ in ($R/t = 600$)

Length, (L) (in)	L/R	λ_{s-k} (lbs/in)	λ_{don} (lbs/in)	λ_{stags} (lbs/in)	Δ_{don} (%)	Δ_{stags} (%)
$[\pm 70/\pm 70/70]_s$ laminate						
90.0	15	29.68	31.31	29.64	−5.2	0.1
60.0	10	30.79	31.91	30.47	−3.5	1.0
40.0	8	30.04	32.94	30.91	−5.7	−2.8
30.0	5	32.31	32.95	31.15	−1.9	3.7
18.0	3	37.81	38.59	37.40	−2.0	1.1
6.0	1	35.08	35.08	32.64	−0.0	3.7
Isotropic						
90.0	15	99.27	101.13	98.56	−1.8	0.7
60.0	10	99.75	100.76	99.93	−1.0	−0.2
40.0	8	100.94	102.39	100.72	−1.4	0.2
30.0	5	101.60	103.05	101.03	−1.4	0.5
18.0	3	102.13	103.45	101.81	−1.3	0.3
6.0	1	101.51	101.51	101.17	−0.0	0.3

Table 5
Buckling loads for curved panel with different L/R ratio, for $t = 0.24$ in and $R = 6.0$ in ($R/t = 25$)

Length (L) (in)	L/R	λ_{s-k} (lbs/in)	λ_{don} (lbs/in)	λ_{stags} (lbs/in)	Δ_{don} (%)	Δ_{stags} (%)
$[\pm 70/\pm 70/70]_s$ laminate						
90.0	15	10,307.9	13,657.3	9903.8	−24.5	4.0
60.0	10	12,000.0	16,000.0	11,579.0	−24.3	3.6
40.0	8	13,625.1	17,303.8	13,016.4	−21.2	4.6
30.0	5	14,430.5	17,754.4	13,742.0	−18.7	5.0
18.0	3	17,284.4	18,709.8	17,214.3	−7.60	0.4
6.0	1	17,320.0	17,330.4	17,132.6	−0.06	1.1
Isotropic						
90.0	15	38,870.1	49,539.4	38,402.8	−21.5	1.2
60.0	10	42,441.8	53,080.6	41,945.4	−20.4	1.1
40.0	8	48,961.8	54,353.0	48,107.3	−9.9	1.8
30.0	5	51,438.7	54,817.2	50,545.6	−6.2	1.7
18.0	3	53,335.1	55,443.4	52,923.4	−3.8	0.7
6.0	1	55,262.0	55,933.1	54,293.2	−1.1	1.7

L/R ratio. For both thin ($R/t = 600$) and thick ($R/t = 25$) panels, Donnell's theory gives good agreement for isotropic and anisotropic panels with small value of L/R ratio.

4. Concluding remarks

The accuracy of Sanders–Koiter, Love and Donnell shell theories for buckling of anisotropic and isotropic curved panel has been assessed. Buckling loads using these shell theories were obtained by using a Rayleigh–Ritz method, where the Ritz functions consist of circulation functions and Legendre polynomials. Comparisons of buckling loads with finite elements results indicate that Sanders–Koiter theory is in good agreement with finite element results and that Love's shell theory is in good agreement with Sanders–Koiter shell theory. Donnell's theory could be in error compared to Sanders–Koiter theory depending on the degree of anisotropy of material and geometrical parameters of the curved panel such as the R/t and L/R ratios.

Results show that differences between buckling loads obtained using the Sanders–Koiter and Donnell shell theories is large for curved panels with small R/t ratios ($R/t \leqslant 100$) where the radius (R) is small. For the same small R/t ratios with large value of radius (R), the difference between buckling loads obtained using Sanders–Koiter and Donnell shell theories is much less than those with the corresponding small R/t ratio with small value of radius. For curved panels with small values of (R/t) ratios and large value of L/R ratios, a large difference in buckling loads is obtained using Sander–Koiter and Donnell theories. This difference is small or negligible for curved panels with small R/t and L/R ratios.

In general, a small or negligible difference is noted in buckling loads obtained using the Sanders–Koiter and Donnell shell theories for curved panels with large R/t ratios. For such panels, only anisotropic material properties seem to affect the difference in buckling loads obtained using the Sanders–Koiter and Donnell shell theories when the L/R ratio is large. As such for most of the cases considered, the difference in buckling loads obtained using the Sanders–Koiter and Donnell shell theories is larger than that for the corresponding case with anisotropic material properties. Since Love's shell theory is in good agreement with Sanders–Koiter shell theory, it is concluded that neglecting the transverse shearing force (Q_y) in the equilibrium of forces in the circumferential direction is mostly responsible for the inaccuracy of Donnell's theory as Love's theory does not include the contribution of the axial and transverse displacement in the twist terms.

Acknowledgements

This work was supported by NASA Grant NAG-1-1588 and is gratefully acknowledged. The authors also appreciate the comments and discussion with Dr David Bushnell from Lockheed-Martin Advanced Technology Center at Palo Alto, California.

Appendix

The types of integrals encountered in the evaluation of the linear and geometric stiffness matrices are

$$\int_{-1}^{+1} R_i R_j \,\mathrm{d}\xi \,\mathrm{d}\eta \tag{18}$$

$$\int_{-1}^{+1} R_{i,\xi} R_j \,\mathrm{d}\xi \,\mathrm{d}\eta \tag{19}$$

$$\int_{-1}^{+1} R_{i,\eta} R_j \,\mathrm{d}\xi \,\mathrm{d}\eta \tag{20}$$

$$\int_{-1}^{+1} R_{i,\xi} R_{j,\xi} \,\mathrm{d}\xi \,\mathrm{d}\eta \tag{21}$$

$$\int_{-1}^{+1} R_{i,\xi} R_{j,\eta} \,\mathrm{d}\xi \,\mathrm{d}\eta \tag{22}$$

$$\int_{-1}^{+1} R_{i,\eta} R_{j,\eta} \,\mathrm{d}\xi \,\mathrm{d}\eta \tag{23}$$

where R_i and R_j can be any of the approximations for u_0, v_0, w_0, ϕ_x, ϕ_y, which are the Ritz functions corresponding to the degrees of freedom of the displacement field for a curved panel in a Rayleigh–Ritz formulation. These integrals correspond to integration over the computational domain. Only the integration scheme for the integral of equation (21) will be discussed herein, since the others are similar.

The integral of eqn (21) can be written as

$$\int_{-1}^{1} R_{i,\xi} R_{j,\xi} \,\mathrm{d}\xi \,\mathrm{d}\eta = \left(\int_{-1}^{1} f(\xi) \,\mathrm{d}\xi\right)\left(\int_{-1}^{1} g(\eta) \,\mathrm{d}\eta\right) = I_\xi I_\eta$$

where

$$I_\xi = \int_{-1}^{1} [(1-\xi)^{p_l}(1+\xi)^{r_l} P_{m_i}(\xi)]_{,\xi} \,[(1-\xi)^{p_t}(1+\xi)^{r_t} P_{m_j}(\xi)]_{,\xi} \,\mathrm{d}\xi$$

$$I_\eta = \int_{-1}^{1} (1-\eta)^{q_l}(1+\eta)^{s_l} P_{n_i}(\eta)(1-\eta)^{q_t}(1+\eta)^{s_t} P_{n_j}(\eta) \,\mathrm{d}\eta \tag{24}$$

since the exponent of the terms $(1\pm\xi)$ and $(1\pm\eta)$ can be either zero or one, eqn (24) can be written as

$$\int_{-1}^{1} [(c_{\xi l}\xi^2 + d_{\xi l}\xi + e_{\xi l}) P_{m_i}(\xi)]_{,\xi} [(c_{\xi t}\xi^2 + d_{\xi t}\xi + e_{\xi t}) P_{m_j}(\xi)]_{,\xi} \,\mathrm{d}\xi$$

$$\times \int_{-1}^{1} (c_{\eta l}\eta^2 + d_{\eta l}\eta + e_{\eta l}) P_{n_i}(\eta)(c_{\eta t}\eta^2 + d_{\eta t}\eta + e_{\eta t}) P_{n_j}(\eta) \,\mathrm{d}\eta = I_{p\xi} I_{p\eta} \tag{25}$$

where the coefficients $c_{\eta l}$, $d_{\eta l}$, $e_{\eta l}$, $c_{\eta t}$, $d_{\eta t}$, $e_{\eta t}$, $c_{\xi l}$, $d_{\xi l}$, $e_{\xi l}$, $c_{\xi t}$, $d_{\xi t}$, and $e_{\xi t}$, depend on the exponents of the terms $(1\pm\xi)$ and $(1\pm\eta)$. After expansion, $I_{p\xi}$ can be written as

$$I_{p\xi}=\int_{-1}^{1}[(a_{\xi l}\xi+b_{\xi l})P_{m_i}(\xi)+(c_{\xi l}\xi^2+d_{\xi l}\xi+e_{\xi l})P'_{m_i}(\xi)]$$
$$\times[(a_{\xi t}\xi+b_{\xi t})P_{m_j}(\xi)+(c_{\xi t}\xi^2+d_{\xi t}\xi+e_{\xi t})P'_{m_j}(\xi)]\,\mathrm{d}\xi \quad (26)$$

Next the properties of Legendre polynomials (see Andrews, 1985) are used to write eqns (25) and (26) in a form more appropriate for analytical integration. The properties of Legendre polynomial ($P_n(v)=P_n$) are

$$P_{-n}=P_{(|n|-1)} \quad (27)$$

$$vP'_n=nP_n+P'_{n-1} \quad (28)$$

$$vP_n=\frac{(n+1)}{(2n+1)}P_{n+1}+\frac{n}{(2n+1)}P_{n-1} \quad (29)$$

$$v^2P'_n=\frac{n(n+1)}{(2n+1)}P_{n+1}+\frac{n^2}{(2n+1)}P_{n-1}+(n-1)P_{n-1}+P'_{n-2} \quad (30)$$

$$v^2P_n=\frac{(n+1)}{(2n+1)}\left\{\frac{(n+2)}{(2n+3)}P_{n+2}+\frac{(n+1)}{(2n+3)}P_n\right\} \quad (31)$$

$$+\frac{n}{(2n+1)}\left\{\frac{n}{(2n-1)}P_n+\frac{(n-1)}{(2n-1)}P_{n-2}\right\} \quad (32)$$

$$P_n=\frac{P'_{n+1}-P'_{n-1}}{(2n+1)} \quad (33)$$

Two other useful properties are

$$\int_{-1}^{1}P_nP_m\,\mathrm{d}v=\begin{cases}0 & \text{for } n\neq m\\ \dfrac{2}{2n+1} & \text{for } n=m\end{cases} \quad (34)$$

$$\int_{-1}^{1}P'_nP'_m\,\mathrm{d}v=\begin{Bmatrix}0 & \text{for } (n+m) \text{ odd}\\ n(n+1) & \text{for } (n+m) \text{ even}\end{Bmatrix}\quad n\leqslant m \quad (35)$$

Hence, eqns (27)–(33) can be used to write $I_{p\xi}$ from eqn (26) as

$$I_{p\xi}=\int_{-1}^{1}\sum_{h=1}^{5}\sum_{s=1}^{5}\alpha_{idh}\alpha_{jdh}P'_{m_{\alpha idk}}P'_{m_{\alpha jfk}}\,\mathrm{d}\xi \quad (36)$$

and eqn (35) is used to evaluate each integral in this summation. Equation (27) is used when Legendre polynomials with negative indices occur. $I_{p\eta}$ from eqn (25) can be written as

$$I_{p\eta} = \int_{-1}^{1} \sum_{h=1}^{5} \sum_{s=1}^{5} \alpha_{ih}\alpha_{jh} P_{m_{\alpha ik}} P_{m_{\alpha jk}} \, \mathrm{d}\eta \tag{37}$$

and eqn (34) is used to evaluate each integral in the above summation. Finally, $I_{p\eta} \times I_{p\xi}$ evaluates integral of the type of eqn (21).

References

Andrews, C.L., 1985. Functions for Engineers and Applied Mathematicians. Macmillan, pp. 116–165.

Bert, C.W., Birman, V., 1988. Parametric instability of thick, orthotropic, circular cylindrical shells. Acta Mechanica 71, 61–76.

Brogan, F.A., Rankin, C.C., Cabiness, H.D., 1994. STAGS User Manual. Lockheed Palo Alto Research Laboratory, Report LMSC P032594.

Brush, D.O., Almroth, B.O., 1975. Buckling of Bars, Plates and Shells. McGraw-Hill.

Chandrashekara, K., Pavan Kumar, D.V.T.G., 1995. Assessment of shell theories for the static analysis of cross-ply laminated circular cylindrical shells. Thin Walled Structures 22, 291–318.

Jaunky, N., Knight, N.F., Ambur, D.R., 1995a. Buckling of arbitrary quadrilateral anisotropic plates. AIAA Journal 33, 938–944.

Jaunky, N., Knight, N.F., Ambur, D.R., 1995b. Buckling analysis of general triangular anisotropic plates using polynomials. AIAA Journal 33, 2414–2417.

Jaunky, N., 1995. Buckling analysis and optimum design of multidirectionally stiffened composite curved panel. Old Dominion University, Norfolk, VA, Ph.D. dissertation.

Jones, M.R., 1975. Mechanics of Composite Materials. McGraw-Hill.

Knight, N.F., Starnes, J.H., 1997. Developments in cylindrical shell stability analysis. Proceedings of the 38th AIAA/ASME/ASC/AHS/ASCE Structures, Structural Dynamics, and Materials Conference, Kissimmee, Florida, April 1997, pp. 1933–1947. Also AIAA Paper No. AIAA-97-1076.

Koiter, W.T., 1959. A consistent first approximation in general theory of thin elastic shells. The theory of thin elastic shells. Proceedings IUTAM Symposium, Delft, North-Holland, Amsterdam, The Netherlands, pp. 12–33.

Leissa, A.W., 1973. Vibration of Shells. NASA SP-288.

Loo, T.T., 1957. An extension of Donnell's equation for circular cylindrical shell. Journal of Aeronautical Sciences 24, 390–391.

Love, A.E.H., 1927. A Treatise on the Mathematical Theory of Elasticity, 4th ed. Dover Publication, New York.

Nemeth, M.P., 1994. Nondimensional parameters and equations for buckling of anisotropic shallow shells. ASME Journal of Applied Mechanics 61, 664–669.

Noor, A.K., 1990. Bibliography of monographs and surveys on shells. Applied Mechanics Review 43 (9).

Park, K.C., Stanley, G.M., 1986. A curved C^0 shell element based on assumed natural-coordinate strains. Journal of Applied Mechanics 53, 278–290.

Sanders, Jr. J.L., 1959. An Improved First Approximation Theory for Thin Shells. NASA Report R-24.

Simitses, G.J., Sheimann, I., Shaw, D., 1985. The accuracy of Donnell's equations for axially-loaded, imperfect orthotropic cylinders. Computers and Structures 20, 939–945.

Stein, M., Neff, J., 1947. Buckling Stresses of Simply Supported Rectangular Flat Plates in Shear. NACA TN 1222.

Stein, M., Batdorf, S.B., 1947. Critical Combinations of Shear and Direct Stresses for Simply Supported Rectangular Flat Plates. NACA TN 1223.

Stein, M., 1986. Nonlinear theory for plates and shells including the effects of transverse shearing. AIAA Journal 24, 1538–1544.

Teng, G.J., 1996. Buckling of thin shells: recent advances and trends. Applied Mechanics Review 49 (4), 263–274.

Yi-Wei, Li, Elishakoff, I., Starnes Jr., J.H., Bushnell, D., 1997. Effect of the thickness variation and initial imperfection on buckling of composite cylindrical shells: asymptotic analysis and numerical results by BOSOR4 and PANDA2. International Journal of Solids and Structures 34, 3755–3767.